FTK51000

Prepared for the
National Institutes of Health
National Institute of Neurological Disorders and Stroke
Neural Prosthesis Program
Bethesda, MD 20892

ELECTRODES FOR FUNCTIONAL NEUROMUSCULAR STIMULATION

Contract #NO1-NS-32300

Quarterly Progress Report #5
1 September, 1994 - 30 November, 1994

Principal Investigator
J. Thomas Mortimer, Ph.D.

Co-Investigator
Warren M. Grill, Ph.D.

Applied Neural Control Laboratory
Department of Biomedical Engineering
Case Western Reserve University
Cleveland, OH 44106

This QPR is being sent to you before it has been reviewed by the staff of the Neural Prosthesis Program

Table of Contents

page

B. Electrode Design and Fabrication

B.2 Electrode Testing: Corrosion Testing of Cuff Electrodes 3

C. Assessment of Electrode Performance in an Animal Model

C.1 Spiral Cuff Electrodes 13

D. Modifications to Improve Functional Performance

D.1b Simulation of Selective Inactivation of Peripheral Fibers 14

Appendix I: Manuscript 15

Section B: Electrode Design and Fabrication

B.2 *Electrode Testing: Corrosion Testing of Cuff Electrodes*

Abstract

To investigate their resistance to corrosion, three 12-contact spiral cuff electrodes were stimulated continuously for 10 weeks while submerged in individual flasks containing phosphate buffered saline solution. Measurements were made over the 10 week period to monitor potential shifts which could signal corrosive events on the surfaces of the contacts. After 10 weeks, the cuffs were removed from the flasks and examined under a dissecting microscope. Initial investigations using scanning electron microscopy have been performed for the contacts of one cuff.

Experimental Set-Up

The experimental set-up was described in detail in a previous progress report (QPR #4). Briefly, three 12-contact spiral cuff electrodes were fabricated according to standard protocol. Each of these cuffs was placed in a small flask containing phosphate buffered saline solution. The flasks were sealed with rubber stoppers and connected through glass tubing to a tank of pure air. Approximately once a week, refreshed pure air was bubble into the flasks. The leads of the electrodes were connected to three stimulator boards programmed to provide a balanced charge rectangular pulse, with 50μs pulsewidth, at a frequency of 20 Hz, and with a recharge limit of approximately 300μA. One tripole of each cuff was not stimulated, and served as a control. Two of the tripoles were stimulated in a tripolar configuration, with current amplitude of 2mA. Current amplitude was set at 1mA for the remaining tripole, which was used for steering (the opposite tripole saw a total of 3mA). Based on the chronic animal studies, these current amplitudes (at 50μs pulsewidths) are at supramaximal levels for nerve recruitment. The stimulation of each of the individual contacts of each cuff are described in Figure 1.

Voltage Measurements

Regular voltage measurements were made for the contacts of each cuff. Initially, these measurements were made between individual contacts and a selected contact in the control tripole. The first four sets of measurements were made in this manner. To obtain more accurate measurements, a saturated calomel reference electrode was used for the remaining three sets of measurements. In both cases, the stimulator boards were turned off during the duration of the measurements.

In the initial measurements, two contacts of a cuff were connected to a stimulator set to generate a sinusoidal current with peak to peak amplitude of 0.1mA at a frequency of 2kHz (in one instance, 10kHz was used). The voltage across the two contacts was displayed on an oscilloscope and the peak to peak amplitude was measured. The same control contact was used for all voltage measurements of a single cuff.

For the measurements using the saturated calomel electrode (SCE) as reference, the same sinusoidal current generator was used, with the current flowing between the contact of interest and one of the control contacts. However, the voltage was measured versus the SCE, not versus the unstimulated control contact that could be experiencing potential shifts of its own. A salt bridge was established between the flask containing the cuff and the beaker of saline in which the SCE was placed. A high impedance differential amplifier (gain of 10, cut-off frequency of 300 Hz) was connected between the SCE and the contact of interest, and the signal was then fed into the oscilloscope for the voltage measurements.

Voltages were divided by the current amplitude to yield the resistance values. The results of these measurements are presented in Figures 2-4. As can be seen, fairly large differences in resistance values were found for measurements made using the control contact. Although all measuurements were increased over the initial (14 days) value, this trend did not continue and resistances increased and decreased from week to week. However, the increases and decreases in resistance were consistent for a specific measurement; i.e., for Cuff B, resistance increased for all contacts from 14 days to 23 days and subsequently they all then decreased at 32 days. This points to the inadequecy of the measurement technique and its susceptibility to perturbations. As could be expected, differences were also seen between the baseline values of the two measurement techniques (voltage measured vs. control contact and vs. SCE).

Although the measurements made using the SCE as reference showed less variation than those made using the control contact as reference, increased resistance values were noted for virtually all of the contacts at 70 days. Because of this, the stimulation was stopped and the cuffs were examined microscopically for evidence of corrosion.

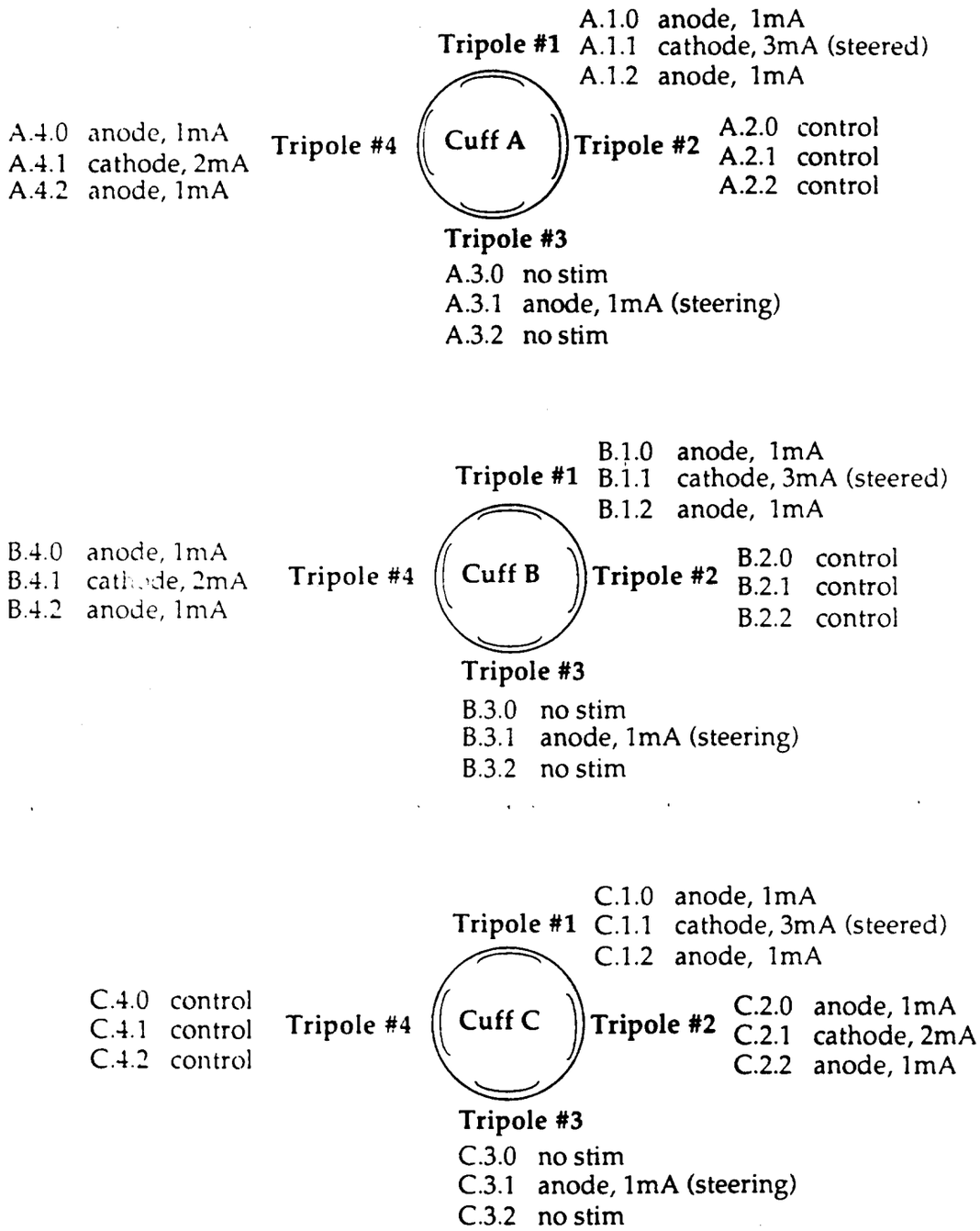

Figure 1: Cross-sectional schematic of the cuffs, with the stimulation and amplitudes of each contact indicated.

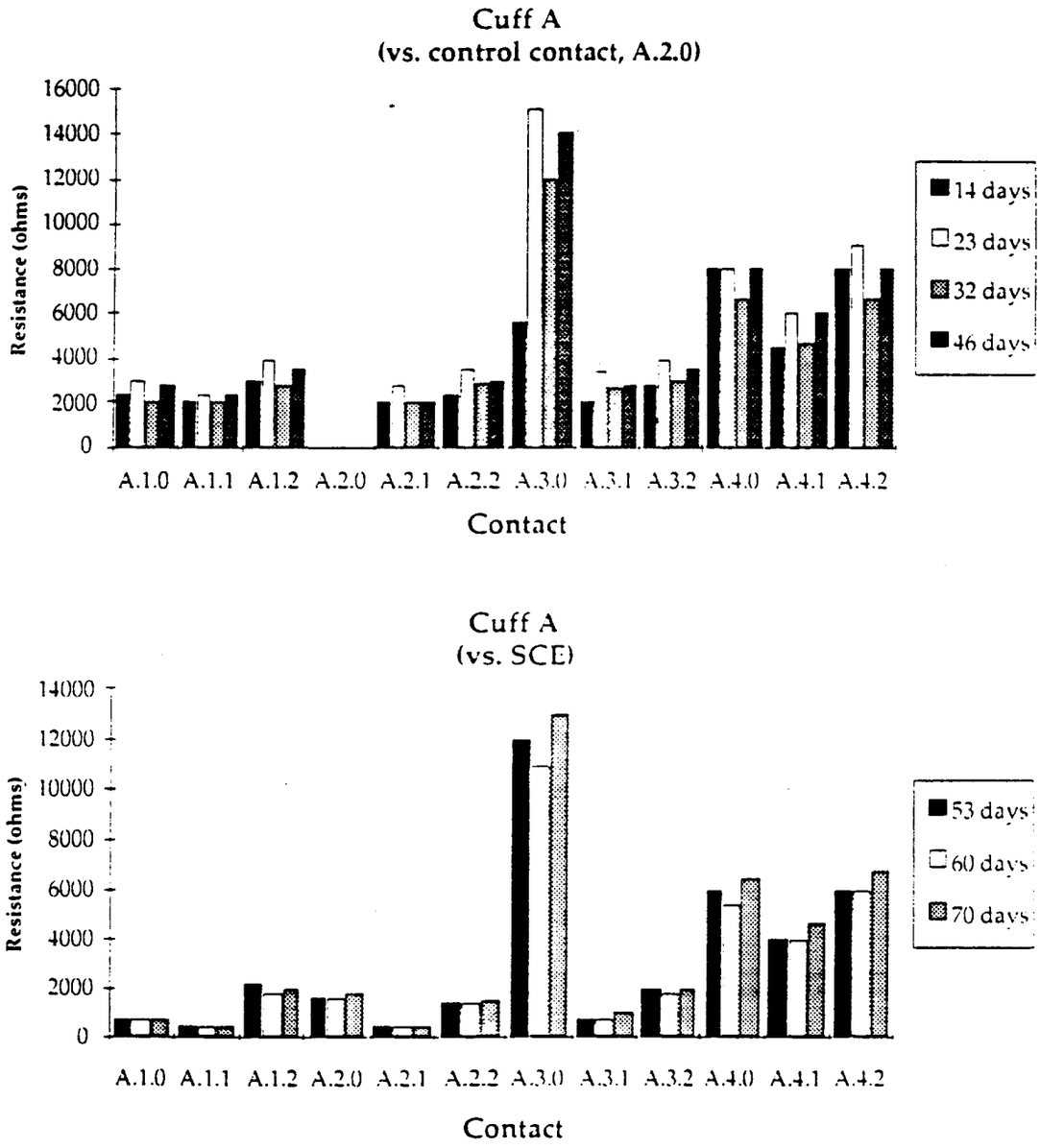

Figure 2: Resistance measurements made for Cuff A. Measurements made using the control contact are presented in the top graph, while those made with the SCE are presented in the lower graph.

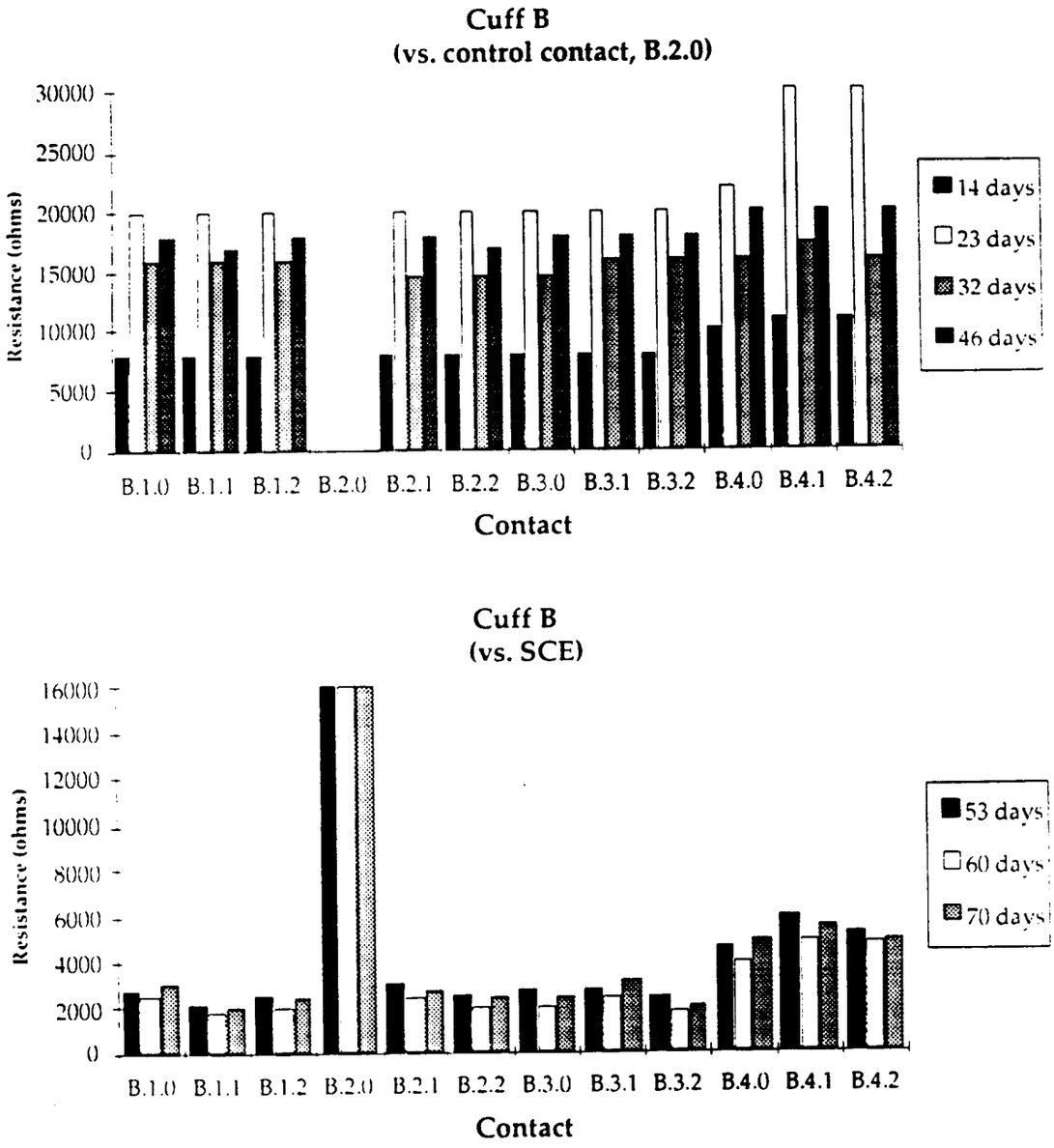

Figure 3: Resistance measurements made for Cuff B. Measurements made using the control contact are presented in the top graph, while those made with the SCE are presented in the lower graph.

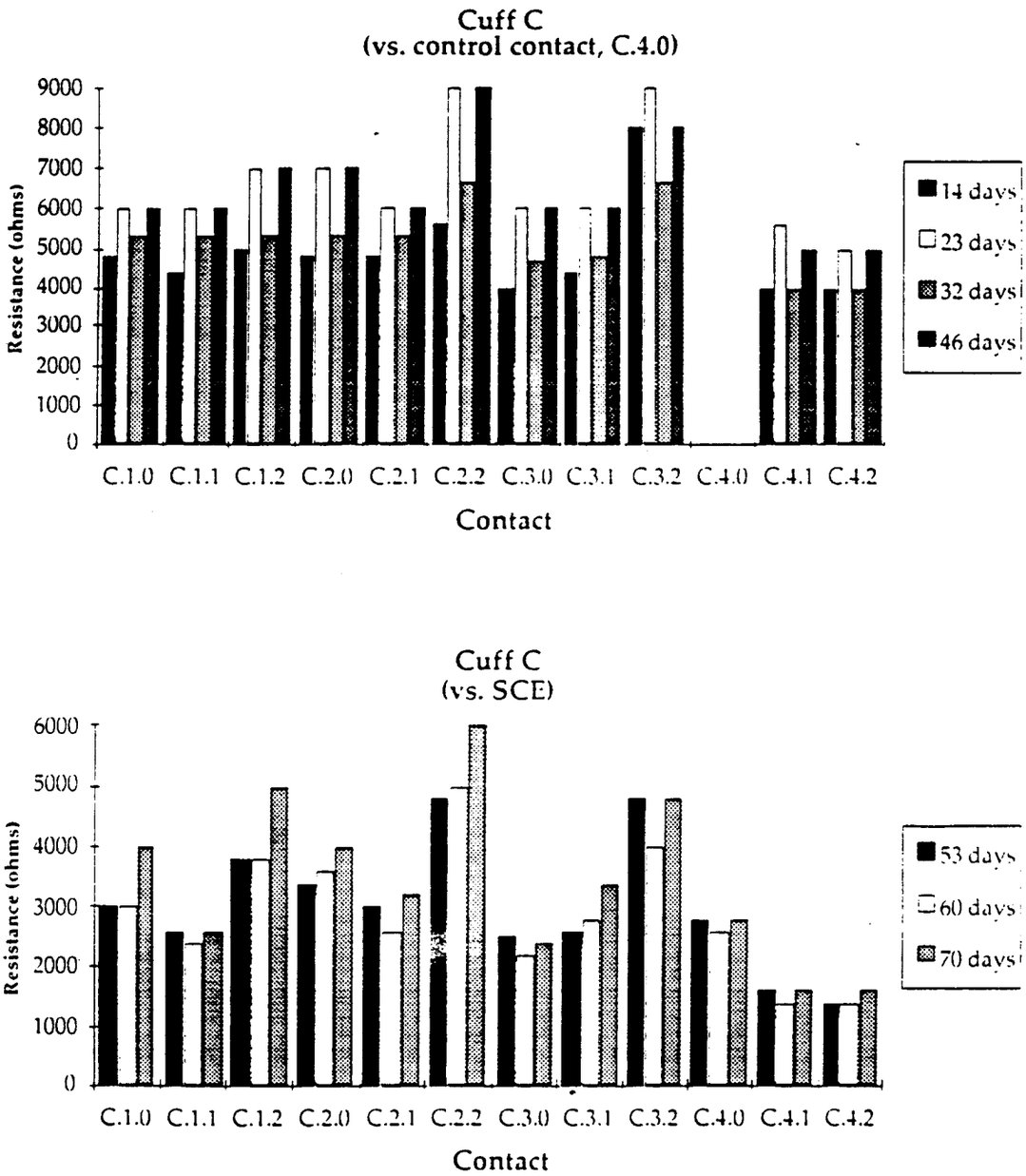

Figure 4: Resistance measurements made for Cuff C. Measurements made using the control contact are presented in the top graph, while those made with the SCE are presented in the lower graph.

Microscopic Examination of Cuffs

Each of the cuffs were examined using a low power dissecting microscope during the initial examination. The contacts of each cuff appeared to have a grainy, matte appearance. This was observed on most contacts of all three cuffs and was not limited to those contacts that had been stimulated.

To further investigate, initial SEM studies have begun on the platinum contacts and stainless steel weld zones. The contacts of Cuff A were cut out of the silicone sheeting using a scalpel blade. Attempts were made to not destroy the weld zone, and to keep a small length of wire attached to the platinum contact. The contacts and wires were then placed on stages for SEM examination. To date, only preliminary studies have been performed.

Striking features seen on the platinum contacts included the presence of large amounts of adherent debris, excessive gouging created by the tool used to cut the window in the silicone sheeting, and frequent score marks. These are presented in Figures 5 and 6.

Isolated, small pits were found on the surface, but were not correlated to either scratches on the surface or to the gouging at the edges of the electrode window. These were seen on both control and stimulated contacts, included the tripolar, steering and steered contacts. In one instance, what appears to be intergranular corrosion was seen throughout a region (Figure 7). However, this instance of corrosion was found on an unstimulated control contact, and cannot be a consequence of the stimulation.

The welds of only three of the contacts have been examined. In two of the cases, only 3 of the 7 strands of wire were included in the weld. Examples of the welds are presented in Figures 8 and 9.

A more complete evaluation will be presented in a future progress report, as the contacts of the remaining two cuffs are being prepared for SEM examination.

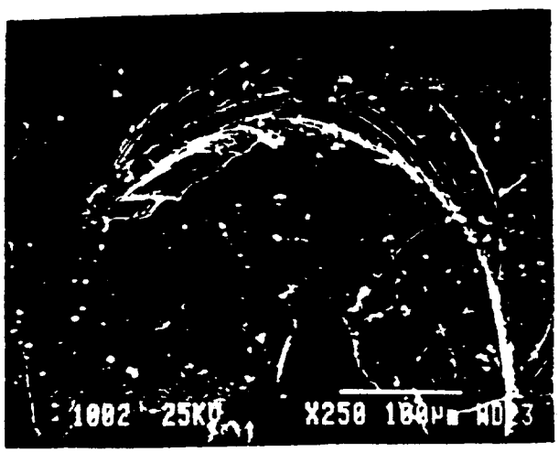

Figure 5: SEM photomicrograph of contact A.2.2. Gouging created by the tool used to cut the window in the silicone sheeting is evident.

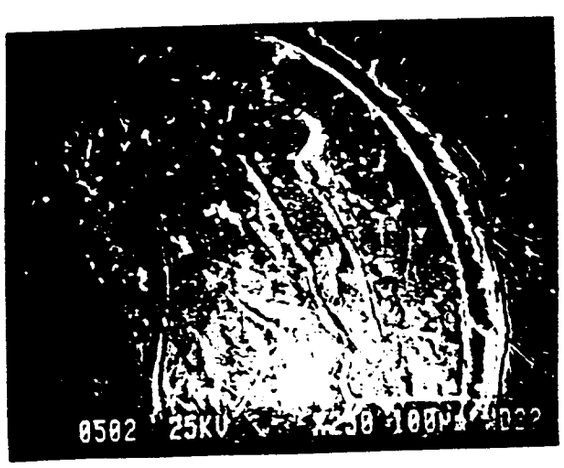

Figure 6: SEM photomicrograph of contact A.1.1. Gouging from the window tool, as well as scoring and surface debris are evident.

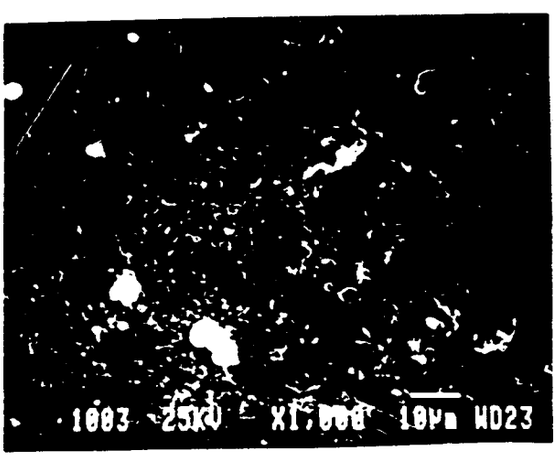

Figure 7: SEM photomicrograph of contact A2.2. Intergranular corrosion can be seen along the central diagonal.

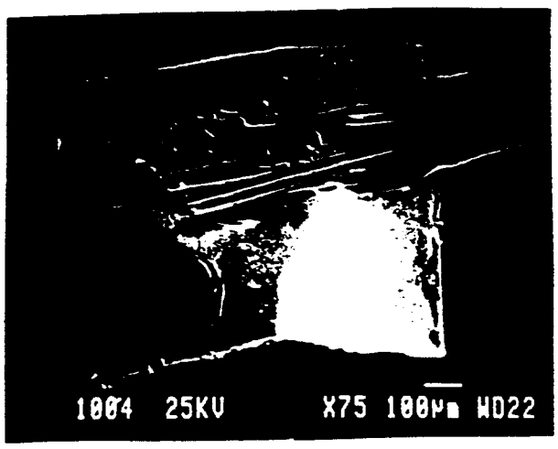

Figure 8: SEM photomicrograph of the weld of contact A.2.0. Two of the wire strands have fractured, and another two strands are not in the weld.

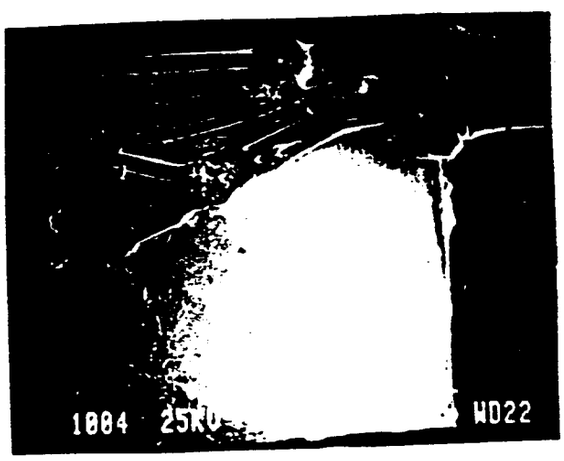

Figure 9: SEM photomicrograph of the weld of contact A.2.2. All strands are welded.

Section C: Quantitative Analysis of Electrode Performance in Acute and Chronic Animals

Spiral Cuff Electrodes

Seven cats have been involved in a chronic study of the 12-contact spiral cuff electrode. In each of these cats, a spiral cuff electrode was implanted on the right sciatic nerve for a period of at least six months. In five of those animals, recruitment data were recorded at regular intervals. These data will be analyzed and reported in a future progress report. To date, three of the animals have been perfused to preserve the tissue, while the remaining animals are scheduled for perfusion in the next quarter. The preserved tissue will be sectioned, embedded, and stained for histologic analysis.

Section D: Modifications to Improve Functional Performance

D.1b Simulation of Selective Inactivation of Peripheral Fibers

Computer simulations and acute animal experiments have been performed to develop a stimulation waveform that inverts the current-distance relationship. In this way, nerve fibers farther from an electrode could be activated without activation of nerve fibers closer to the electrode. Enclosed is a manuscript, submitted to the journal *Brain Research* , reporting on this work.

Appendix I

Inversion of the Current-Distance Relationship by Transient Depolarization

Warren M. Grill and J. Thomas Mortimer

submitted to *Brain Research*

INVERSION OF THE CURRENT-DISTANCE RELATIONSHIP BY TRANSIENT DEPOLARIZATION

Warren M. Grill and J. Thomas Mortimer

Applied Neural Control Laboratory
Department of Biomedical Engineering
Case Western Reserve University
C.B. Bolton Bldg., 3480
Cleveland, OH 44106-4912

phone (216) 368-2960
fax (216) 368-4872

email:
wmg@po.cwru.edu
jtm3@po.cwru.edu

ABSTRACT

The objective of this research was to develop a stimulus waveform to effect excitation of nerve fibers distant from an electrode without excitation of nerve fibers close to the electrode. Models of mammalian peripheral myelinated axons and experimental measurements on cat sciatic nerve were used to determine the effects of sub-threshold depolarization on neuronal recruitment by electrical current stimuli. The shape of the stimulus current waveform was designed to take advantage of the non-linear conductance properties of neuronal sodium channels to control neuronal excitability. Sub-threshold membrane depolarization generated a transient decrease in neuronal excitability and thus an increase in the threshold for stimulation by a subsequent stimulus pulse. The decrease in excitability increased as the duration and amplitude of the sub-threshold depolarization were increased, and the increase in threshold was greater for fibers close to the electrode. When a depolarizing stimulus pulse was applied immediately after the sub-threshold depolarization, nerve fibers far from the electrode could be stimulated without stimulating fibers close to the electrode. Thus, sub-threshold depolarizing pre-pulses inverted the current-distance relationship, and allowed selective stimulation of nerve fibers far from the electrode.

Key Words: electrical stimulation, nerve stimulation, current-distance relationship, sodium inactivation, stimulus waveform, electrode

INTRODUCTION

Selective stimulation of neurons within the central and peripheral nervous systems is a powerful tool to study neural function and a requirement for multi-channel neural prosthetic devices [12]. For example, stimulation of discrete populations of cochlear nerve fibers allows exploitation of the tonotopic map of the cochlea in cochlear prostheses [2, 21], and selective stimulation of peripheral nerve fascicles allowed independent control of the contraction strength generated in individual skeletal muscles innervated by a common nerve trunk [23, 26]. Electrode designs presently under development for selective stimulation of peripheral nerve trunk fascicles include multiple contact nerve cuff electrodes [26], intrafascicular wire electrodes [28], intrafascicular silicon electrodes [18], and wire electrodes sutured to the epineurium [24].

Nerve-based electrode designs share the common goal of stimulating a discrete region of a peripheral nerve trunk. Selectivity has been accomplished by placing multiple, spatially distributed electrode contacts in or on different regions of a nerve trunk. Using conventional stimuli (e.g., 100usec rectangular current pulses) nerve fibers lying closer to an electrode are recruited at lower current amplitudes than required to excite more distant fibers. The threshold current for excitation of myelinated nerve fibers is proportional to the square of the distance from the electrode to the nerve fiber [16]. Thus, proximity of the electrode to the nerve fibers targeted for activation has been the primary means to achieve selectivity.

Along with electrode geometry, the choice of stimulus waveform can also affect neuronal selectivity. Short duration current pulses increase the threshold difference between nerve fibers of different diameters, and thus produce more easily graded muscle contractions [6]. Modeling and experimental studies have demonstrated that a secondary stimulus phase, used for charge recovery, can abolish action potentials in nerve fibers excited just above threshold. The abolition of action potentials depended on the shape, amplitude, and duration of the secondary phase and was eliminated by an interphase delay [25]. More recently, we have demonstrated that short stimulus pulsewidths increase the slope of the current-distance-relationship, thus increasing the threshold difference between nerve fibers at different distances from the electrode [8]. Thus, for a particular

electrode geometry, the choice of stimulus parameters affects the population of nerve fibers that will be stimulated.

The objective of this research was to develop stimulation waveforms to effect excitation of nerve fibers distant from an electrode without excitation of nerve fibers close to the electrode. Such a technique would allow selective stimulation of nerve fibers lying deep in a nerve trunk without the risk of neural damage associated with electrodes that penetrate the nerve trunk [19]. Stimulus waveforms were designed to invert of the slope of the current-distance relationship by exploiting the non-linear conductance properties of the neural membrane. Inversion of the current-distance relationship allowed stimulation of fibers lying more distant from an electrode at lower currents than required to stimulate fibers lying close to the electrode. Preliminary results of this study have been published in abstract form [9].

METHODS

INSERT FIGURE 1 HERE

Computer Simulations with a Single Node Model

A model of a space-clamped patch of mammalian neural membrane was used to study the effects of sub-threshold transmembrane depolarization on neuronal excitability. The membrane patch was modeled based on voltage clamp studies of rabbit peripheral myelinated nerve fiber membrane [22]. The model included a non-linear sodium conductance, a linear leakage conductance, and membrane capacitance (fig. 1A). The first order differential equation describing the transmembrane potential [14] was solved using a second-order predictor corrector algorithm [5] implemented in PASCAL. A 2 msec simulation that computed and displayed transmembrane potential, transmembrane currents, and the values of the ion channel gating parameters took less than 3 sec. to run on a Macintosh Quadra 950. The effects of sub-threshold membrane depolarization were studied by determining the threshold amplitude for excitation with different combinations of depolarizing pre-pulse (DPP) amplitude, DPP duration, interphase delay, and stimulus duration.

Computer Simulations of Myelinated Nerve Fiber Recruitment

A computer model of a mammalian myelinated nerve fiber was used to determine the effects of sub-threshold depolarizing pre-pulses (DPPs) on the current-distance relationship. Nerve fibers were modeled using a 21 compartment cable model (fig. 1B) with the nodes of Ranvier described by mammalian non-linear membrane kinetics [22] and the myelin was assumed to be a perfect insulator [13]. All model parameters and assumptions were the same as those of Warman et al. [27]. The first order non-linear differential equation describing the transmembrane voltage at each node was solved using the fourth-order Runge-Kutta method with doubling and halving of the time step [5] implemented in FORTRAN [22].

The model nerve fiber was positioned at different distances (0.25-1.5 mm) from a point current source positioned above the middle compartment of the cable in a homogeneous, isotropic medium (ρ=55 Ω-cm). An iterative method was used to determine threshold current (±1%) to

generate propagating action potentials in 10μm and 20 μm diameter nerve fibers with rectangular constant current pulses. A simulation run to determine the threshold current for one fiber configuration took approximately 2 min. on a Gateway 486/25. Criteria to recognize a propagating action potential were transmembrane voltage that exceeded 0 mV and a rate of change in transmembrane voltage that exceeded 60 mV/ms at a node 5 internodal lengths from the central node of the cable. The threshold amplitude for excitation with the stimulus pulse was determined as a function of the electrode to fiber distance for different combinations of pre-pulse amplitude, pre-pulse duration, and stimulus duration.

Experimental Measurements of Nerve Fiber Recruitment

Experiments were conducted in an animal model to determine the effects of sub-threshold DPPs on the recruitment properties of direct nerve stimulation. All animal care and experimental procedures were according to NIH guidelines and were approved by the Institutional Animal Care and Use Committee of Case Western Reserve University. Silicone rubber spiral nerve cuff electrodes, containing 12 individually addressable platinum electrode contacts [26], were implanted on the right sciatic nerve of adult cats. In this report, data are included from 3 acute experiments and 5 chronic experiments.

In acute experiments, animals were initially anesthetized with ketamine hydrochloride (35 mg/kg, I.M.), and atropine sulfate (0.05 mg/kg, I.M.) was administered to reduce salivation. Animals were intubated, a catheter was inserted in the cephalic vein, and a surgical level of anesthesia was maintained throughout the experiment with sodium pentobarbital (5-10 mg bolus injections, I.V.). For measurements with chronically implanted nerve cuff electrodes, animals were initially anesthetized with xylazine (Rompun, 2.0 mg/kg, SQ), masked with 3.0% gaseous Halothane in O_2, intubated, and maintained at a surgical level of anesthesia with 1.5-2.0% gaseous Halothane in O_2. During both acute and chronic measurements, body temperature saline was administered (10 cc/kg/hour) during the testing interval, body temperature was maintained with a heating pad, and heart rate and respiratory rate were continuously monitored.

Animals were mounted in a stereotaxic apparatus to measure the 3-dimensional isometric torque generated at the ankle joint by stimulation of the sciatic nerve [7]. Twitch contractions in the ankle musculature were generated using controlled current rectangular pulses applied at 0.5 Hz. Monopolar electrode configurations where one contact in the cuff acted as the cathode and a 1.5 in. 22 gage subcutaneous needle acting as the anode, and longitudinal tripolar electrode configurations with a dot cathode between two dot anodes within the cuff were used [26]. The amplitude and duration of the pre-pulse were selected to be sub-threshold, and the amplitude of the stimulus was stepped between threshold and maximum to generate recruitment curves of torque as a function of stimulus current amplitude using different depolarizing pre-pulses. An interleaved stimulus paradigm, where stimuli with and without the pre-pulse were applied alternately, was employed to avoid any time dependent changes (e.g., fatigue) that might affect the data. Stimulus amplitude was set manually with calibrated potentiometers while stimulus pulsewidth was controlled by the computer. The applied current waveform was monitored on a storage oscilloscope by differentially measuring the voltage generated in a 100Ω resistor in series with the electrodes.

Stimulus control and response sampling were done using a multiple function input output board (NB-MIO-16H, National Instruments) in a Macintosh Quadra 950 and were controlled using software written in LabView (National Instruments). The torque signals were low pass filtered at 100 Hz and sampled at 200 Hz with a 12-bit A/D converter. Five to ten twitch responses were collected at each stimulus amplitude and were averaged. The peak of the average torque twitch waveform was used as the measure of activation at each stimulus amplitude [7].

RESULTS

INSERT FIGURE 2 HERE

Effects of Sub-threshold Depolarization on Neuronal Excitability

Space Clamped Node of Ranvier

The effect of sub-threshold membrane depolarization on the threshold current amplitude for a subsequent stimulus was studied using a model of a patch of mammalian neuronal membrane. Sub-threshold depolarizing pre-pulses (DPPs) decreased neuronal excitability and thus increased threshold for generation of an action potential by subsequent stimuli.

The transmembrane voltage response of a membrane patch to the two-pulse paradigm is shown in fig. 2. The amplitude of the pre-pulse in this example (1200μA/cm^2) was equal to 90% of the excitation threshold for a 500μsec duration pulse. As the delay between the sub-threshold DPP and application of the stimulus was increased (from A to C), the threshold for activation increased. The stimulus (100μsec, 1460μA/cm^2) was sufficient to generate an action potential when applied at the onset of the DPP (fig. 2A). When the same stimulus was applied 200μsec after the onset of the DPP, it was just supra-threshold (fig. 2B). The latency for generation of the action potential is much larger in fig. 2B than in fig. 2A indicating that the stimulus in fig. 2B. is just supra-threshold [14]. When the stimulus was applied 400μsec after the onset of the DPP it did not generate an action potential (fig. 2C). At this point the DPP had elevated threshold beyond the amplitude of the stimulus pulse. If the same stimulus was applied 500μsec after the cessation of the DPP, it again generated an action potential (fig. 2D). Thus, sub-threshold depolarization generated a transient decrease in neuronal excitability, and thus caused a transient increase in the threshold for stimulation.

INSERT FIGURE 3 HERE

The effect of sub-threshold membrane depolarization on excitability varied with the duration and amplitude of the DPP, the delay between the DPP and the stimulus, as well as the duration of the stimulus (fig. 3). Short duration (≤100μsec) DPPs decreased, rather than increased, threshold for stimuli of all durations that were tested (see below). Longer duration

DPPs increased threshold, and the magnitude of the increase varied with the duration of the stimulus pulse. Long duration DPPs coupled with long duration stimuli generated the maximal increases in threshold (fig. 3A). The increases in threshold generated by DPPs increased progressively as the amplitude of the DPP was increased from 5% of the excitation threshold to 95% of the excitation threshold (fig. 3B). Similarly, the effects of DPPs decayed progressively as the interphase delay between the pre-pulse and the stimulus was increased from 0 to 1000μsec (fig. 3C). Thresholds returned to those measured without any pre-pulse 500μsec after cessation of the pre-pulse. Thus, maximal decreases in excitability were generated for long DPPs with just sub-threshold amplitudes followed at 0 delay by stimulus durations of 100μsec or longer.

INSERT FIGURE 4 HERE

Cat Sciatic Nerve Fibers

The effect of sub-threshold DPPs on threshold for stimulation of cat sciatic nerve motor fibers was measured. Long duration DPP decreased neuronal excitability, thus increasing threshold for subsequent stimulation. The magnitude of the increase in threshold varied with the duration of the DPP. The increase in threshold generated by 500μsec DPPs, with amplitude equal to 90-95% of the excitation threshold, ranged from 8-340% of the threshold without any pre-pulse (77±117%, mean±S.D., n=17) while increases in threshold generated by 1000μsec DPPs, with amplitude equal to 90-95% of the excitation threshold, ranged from 25-78% of the threshold without any pre-pulse (54±22%, n=7). Longer duration DPPs generated larger increases in threshold for subsequent stimulation (fig. 4A). The magnitude of the increases in threshold also varied with the relative amplitude of the pre-pulse. Larger amplitude pre-pulses generated larger increases in threshold (fig. 4B). Thus, sub-threshold depolarizing pre-pulses increased the threshold for activation of cat sciatic nerve motor fibers, and the magnitude of threshold elevation varied with the pre-pulse parameters as predicted by the model.

INSERT FIGURE 5 HERE

Mechanism for Increases in Threshold

The values of the sodium channel gating parameters [11], **m** and **h**, were tracked (fig. 5) during the application of DPPs to illustrate the mechanism for the decreases in neuronal excitability (see [14] for a review of the Hodgkin Huxley description of neuronal excitability). The sodium channel activation parameter, **m**, increases (i.e., the channel opens) in response to transmembrane depolarization, and decreases (i.e., the channel closes) in response to transmembrane re-polarization [11]. The sodium channel inactivation parameter, **h**, decreases (i.e., the inactivation gate closes) in response to transmembrane depolarization, and increases (i.e., the inactivation gate opens) in response to transmembrane re-polarization [11]. Thus, membrane potential has the dual effect of both increasing and decreasing membrane conductance [10]. The time constant of channel activation, τ_m, is an order of magnitude smaller than the time constant of channel inactivation, τ_h [1, 15]. Furthermore, the inactivation parameter, **h**, has a much steeper voltage dependence for small depolarizations from rest than does the activation parameter, **m** [1].

The transmembrane potential and the values of the gating parameters during a sub-threshold DPP followed by the same amplitude stimulus pulse either 100μsec (fig. 5A) or 400μsec (fig. 5B) after the onset of the stimulus pulse are shown in fig. 5. During the pre-pulse, the value of **h** was decreased at a constant rate, while the value of **m** increased rapidly to a plateau value slightly above the rest value.

Short duration DPPs caused an increase in excitability (fig. 3A) as a result of the long time constant of the sodium inactivation gate. During a short (100μsec) DPP (fig. 5A), the rapidly changing activation parameter, **m**, increases (**m** increased by 1017% and $\mathbf{m^2}$ increased by 12,368%), but the inactivation parameter, **h**, does not have time to decrease sufficiently to cause elevation in threshold (**h** decreased by 17%). Thus, short duration depolarizations lead to an increase, rather than a decrease, in excitability.

Long duration DPPs caused a decrease in excitability (fig. 3B) by inactivation of the sodium channels. For long duration membrane depolarizations (400μsec), the value of **h** decreased significantly (-50%), while the value of **m** decreased relative to the increases at 100μsec

(fig. 5B). Between 100μsec and 400μsec **m** decreased by 6% and $\mathbf{m^2}$ decrease by 12%. The result was a net decrease in neuronal excitability and an increase in threshold for subsequent stimuli.

INSERT FIGURE 6 HERE

Effect of Pre-Pulses on Neuronal Recruitment

Inversion of the Current-Distance Relationship

Cable models of 10μm and 20μm mammalian myelinated nerve fibers were used to study the effect of DPPs on the relationship between the threshold current and the distance between the electrode and the nerve fiber. With single 500μsec rectangular stimuli, the threshold current increased as the square of the distance between the electrode and the nerve fibers (fig. 7A). Furthermore, stimulation of smaller diameter nerve fibers (10 μm) required larger stimulus amplitudes than stimulation of larger diameter nerve fibers (20 μm).

Application of a sub-threshold DPP before the stimulus elevated threshold for fibers close to the electrode. The increase in threshold was sufficient to allow stimulation of fibers lying more distant from the electrode at lower currents than required to stimulate fibers close to the electrode. The transmembrane potential at 3 nodes of two 20μm model nerve fibers positioned 0.25mm and 0.5mm from the electrode is shown in fig. 6. The applied current waveform was a 500μsec DPP with an amplitude (124μA) equal to 90% of the threshold for the fiber at 0.25mm followed by a 500μsec stimulus pulse. The DPP generated a sub-threshold depolarization in both fibers, but the magnitude of the depolarization was larger in the closer fiber. The difference in depolarization caused a larger decrease in excitability of the fiber at 0.25mm than the fiber at 0.5mm. Thus, the subsequent stimulus pulse generated a propagating action potential in the fiber at 0.5 mm, but not in the fiber at 0.25mm. The DPP allowed stimulation of a fiber positioned further from the electrode at a lower current amplitude than required to excite the fiber closer to the electrode.

INSERT FIGURE 7 HERE

The current-distance relationship for 10μm and 20μm nerve fibers after a 500μsec depolarizing pre-pulse with an amplitude equal to 95% of the excitation threshold for the 20μm

fiber at 0.25mm is shown in fig. 7. The DPP inverted the slope of the current-distance curve in the proximity of the electrode. The 20μm fibers 0.5mm and 0.75mm from the electrode, and the 10μm fibers 0.5mm from the electrode, were stimulated at lower current amplitudes than required to stimulate the fibers 0.25mm from the electrode. DPPs thus allowed selective stimulation of fibers lying more distant from the electrode at lower current amplitudes than required to excite fibers close to the electrode.

A stepped pre-pulse waveform was used to inactivate further fibers lying close to the electrode, and stimulate selectively even more distant nerve fibers (fig. 7C). The first pre-pulse elevated threshold for the closest fibers as seen above. A second DPP of a larger amplitude was then applied without generating excitation in the closest fibers, because their threshold had been elevated by the first pulse. The second step of the pre-pulse further elevated threshold for fibers close to the electrode, and inverted the current-distance curve over a larger distance than did the single DPP. The 10μm fibers between 0.75mm and 1.5mm, and the 20μm fibers between 1.0mm and 1.5mm, were stimulated at lower currents than fibers closer to the electrode. Stepped pre-pulse waveforms caused inversion of the current-distance curve over a larger region, and thus allowed selective activation of fibers even more distant from the electrode.

Using the stepped pre-pulse waveform, the threshold of the 20μm fiber at 0.25mm was elevated by more than 7 times and thus action potential propagation in these fibers was blocked by hyperpolarization of the adjacent nodes. Also, in two cases, the site of initiation of the action potential shifted from the central node of the cable to the nodes that flanked the central node (10μm fiber 0.5mm from the electrode and 20μm fiber 0.75mm from the electrode). In these cases, the central node was inactivated to a degree that threshold was lower for excitation of the flanking nodes.

The stepped pre-pulse also allowed stimulation of small nerve fibers at lower stimulus amplitudes than large nerve fibers (i.e., natural recruitment order) at 0.75mm from the electrode (fig. 7C). This was not unexpected since extracellular electric fields, whether stimulating or inactivating, affect large nerve fibers to a greater degree than small nerve fibers. The DPP created a

larger sub-threshold depolarization in the large fibers and thus a greater degree of inactivation of the sodium conductance. There was thus a differential increase in threshold in the 20μm fibers relative to the 10μm fibers, and the 10μm fibers were stimulated at a lower current amplitude than the 20μm fibers.

INSERT FIGURE 8 HERE

Experimental Example

The model results demonstrating inversion of the current-distance relationship suggested that DPPs could be used to stimulate first a fascicle that was stimulated second with conventional stimuli. An example of selective activation of the second recruited fascicle using a 500μsec DPP with amplitude (40μA) equal to 90% of the excitation threshold is shown in fig. 8. Without a pre-pulse, the active electrode first generated plantarflexion torques as indicated by the positive deflection in the recruitment curve and the positive going twitch waveforms. As the stimulus amplitude was further increased, the stimulus spread to excite the innervation of the muscles producing dorsiflexion at the ankle joint (i.e., the common peroneal fascicle of the sciatic nerve). This was seen as a decrease in the net torque at the joint and a negative deflection in the torque twitch waveform at 65μA (arrow in fig. 8).

When a 500μsec depolarizing pre-pulse preceded the stimulus, dorsiflexion torques were generated at smaller current amplitudes than were plantarflexion torques. This was seen as a negative deflection in the recruitment curve and the negative going twitch waveforms. As the stimulus amplitude was increased, excitation spread to excite the innervation of the plantarflexor muscles. Thus, the pattern of torques generated using the DPP was the inverse of the pattern of torques generated using conventional rectangular stimuli. These data demonstrate that depolarizing pre-pulses allowed stimulation of the second recruited fascicle (common peroneal fascicle in this example) before activation of the first recruited fascicle. This provides experimental evidence indicating inversion of the current-distance relationship using sub-threshold DPPs.

DISCUSSION

The results of this study demonstrate how the non-linear conductances of neural membrane can be controlled to alter neuronal recruitment. Selective inactivation of fibers close to an electrode by sub-threshold depolarizing pre-pulses elevated their threshold for subsequent stimulation. This had the effect of inverting the current-distance relationship close to the electrode which allowed fibers that were further from the electrode to be stimulated at currents smaller than required to stimulate fibers close to the electrode. Computer simulations of the effect of pre-pulse and stimulus parameters indicated that maximal decreases in excitability were generated for long DPPs with just sub-threshold amplitudes followed at 0 delay by stimulus durations of at least 100μsec. Experimental measurements on the cat sciatic nerve supported the predictions made with the computer model, and demonstrated activation first of a fascicle that was recruited second using conventional rectangular stimuli.

Sub-threshold depolarization decreased neuronal excitability by inactivation of the voltage dependent sodium channel. Membrane depolarization both increases sodium conductance by opening the membrane pore and decreases sodium conductance by closing the inactivation gate [10]. The difference in the time constants between pore opening and gate closing and the differences in the voltage dependent of the activation and inactivation parameters are what leads to the action potential, and what allowed selective inactivation of closer nerve fibers. The state of inactivation produced by sub-threshold membrane depolarization is analogous to the refractory period present after generation of an action potential.

Modeling results with the stepped DPP indicated that DPPs allow selective stimulation of small nerve fibers at lower currents than required for stimulation of large nerve fibers. Previous investigators have documented this effect of membrane depolarization. Zimmerman [20, 29] used very long duration (hundreds of milliseconds to seconds) depolarizing pre-pulses to achieve differential block of large diameter nerve fibers and thus stimulate selectively small diameter nerve fibers. Similarly, Fukushima et al. [4] used very slowly rising current ramps to block differentially small caliber nerve fibers by membrane depolarization. The charge injection required

to achieve this effect with the reported waveforms, however, was very large. Charge injection for chronic neural prosthetic applications is limited by the requirement that the electrode not be corroded and the underlying tissue not be damaged [17]. Furthermore, very long duration pulses will preclude repetitive activation at the 10-50 Hz frequencies required for motor prosthetic applications. Another method to achieve selective activation of small nerve fibers is arrest of conduction in large nerve fibers by anodal block [3]. The long-duration quasi-trapezoidal waveforms used in this technique must have an amplitude several times larger than threshold to cause anodal block. Thus this method also requires large charge injection for efficacy. Model results indicate that the stepped pre-pulse waveforms described in this study allow selective activation of small fibers using less total injected charge.

ACKNOWLEDGMENTS

The authors thank Drs. D. Durand, P.H. Peckham, and R.E. Ritzmann for critically reading an earlier version of this manuscript.

The authors thank Ms. N. Caris, Ms. J. Crossen, and Mr. D. Tyler for assistance during the animal experiments, Mr. H. Kayyali for fabrication and maintenance of the laboratory stimulator, and Mr. M. Miller for development of the data collection software.

The software for the model of the space clamped membrane patch was written by Mr. D.G. Atzberger and Mr. Z.H. Munir. The software for the fiber model was obtained from Dr. D.H. Perkel and modified by Drs. J.D. Sweeney and E.N. Warman.

This work was supported in part by a grant from the Paralyzed Veterans of America Spinal Cord Research Foundation and by NIH NINDS Neural Prosthesis Program Contract N01-NS-3-2300.

REFERENCES

[1.] Chiu, S.Y., Ritchie, J.M., Rogart, R.B., Stagg, D., A quantitative description of membrane current in rabbit myelinated nerve, J. Physiol., 292 (1979) 149-166.

[2.] Clark, G.M., Black, R., Dewhurst, D.J., Forster, I.C., Patrick, J.F., Tong, Y.C., A multiple-electrode hearing prosthesis for cochlear implantation in deaf patients, Med. Prog. Technol., 5 (1977) 127-140.

[3.] Fang, Z.-P., Mortimer, J.T., Selective activation of small motor axons by quasitrapezoidal current pulses, IEEE Trans. Biomed. Eng., 38 (1991) 168-174.

[4.] Fukushima, K, Yahara, O., Kato, M., Differential blocking of motor fibers by direct current, Pflügers Arch., 358 (1975) 235-242.

[5.] Glantz, S.A., Mathematics for Biomedical Applications. Univer. of Calif. Press, Berkeley, 1979, pp. 310-321.

[6.] Gorman, P.H., Mortimer, J.T., Effect of stimulus parameters on recruitment with direct nerve stimulation, IEEE Trans. Biomed. Eng. 30 (1986) 407-414.

[7.] Grill, W.M., Mortimer, J.T., Non-invasive measurement of the input output properties of peripheral nerve stimulating electrodes, submitted to J. Neuroscience Methods.

[8.] Grill, W.M., Mortimer, J.T., Effect of stimulus pulsewidth on spatial selectivity of neural stimulation, Proc. 16th Int. Conf. IEEE-EMBS, 16 (1994) 363-364.

[9.] Grill, W.M., Mortimer, J.T., Selective activation of distant nerve fibers. Proc. 15th Int. Conf. IEEE-EMBS, 15 (1993) 1259-1250.

[10.] Hodgkin, A.L., Huxley, A.F., The dual effect of membrane potential on sodium conductance in the giant axon of Loligo, J. Physiol., 116 (1952) 497-506.

[11.] Hodgkin, A.L., Huxley, A.F., A quantitative description of membrane current and its application to conduction and excitation in nerve, J. Physiol., 117 (1952) 500-544.

[12.] Loeb, G.E., Neural prosthetic interfaces with the nervous system, Trends in Neurosci., 12 (1989) 195-201.

[13.] McNeal, D.R., Analysis of a model for excitation of myelinated nerve, IEEE Trans. Biomed. Eng., 23 (1976) 329-337.

[14.] Mortimer, J.T., Electrical excitation of nerve. In W.F. Agnew, D.B. McCreery (Eds.), Neural Prostheses: Fundamental Studies, Prentice Hall, Englewood Cliffs, New Jersey, 1990, pp. 67-84.

[15.] Neumke, B., Schwarz, J.R., Stampfli, R., A comparison of sodium currents in rat and frog myelinated nerve: normal and modified sodium inactivation, J. Physiol., 382 (1987) 175-191.

[16.] Ranck, J.B., Jr., Which elements are excited in electrical stimulation of mammalian central nervous system: a review, Brain Res., 98 (1975) 417-440.

[17.] Robblee, L.S., Rose, T.L., Electrochemical guidelines for selection of protocols and electrode materials for neural stimulation. In W.F. Agnew, D.B. McCreery (Eds.), Neural Prostheses: Fundamental Studies, Prentice Hall, Englewood Cliffs, New Jersey, 1990, pp. 25-66.

[18.] Rutten, W.L.C., van Wier, H.J., Put, J.H.M., Sensitivity and selectivity of intraneural stimulation using a silicon electrode array, IEEE Trans. Biomed. Eng., 38 (1991) 192-198.

[19.] Rydevik, B.L., Danielsen, N., Dahlin, L.B., Lundborg, G., Pathophysiology of peripheral nerve injury with special reference to electrode implantation. In W.F. Agnew, D.B. McCreery (Eds.), Neural Prostheses: Fundamental Studies, Prentice Hall, Englewood Cliffs, New Jersey, 1990, pp. 85-105.

[20.] Sassen, M, Zimmermann, M., Differential blocking of myelinated nerve fibers by transient depolarization, Pflügers Arch., 341 (1973) 179-195.

[21.] Schindler, R.A., Merzenich, M.M. (Eds.), Cochlear Implants, Raven Press, New York, 1985.

[22.] Sweeney, J.D., Durand, D., Mortimer, J.T., Modeling of mammalian myelinated nerve for functional neuromuscular stimulation, Proc. 9th Int. Conf. IEEE-EMBS, 9 (1987) 1577-1578.

[23.] Sweeney, J.D., Ksienski, D.A., Mortimer, J.T., A nerve cuff technique for selective excitation of peripheral nerve trunk regions, IEEE Trans. Biomed. Eng., 37 (1990) 706-715.

[24.] Thoma, H., Girsch, W., Holle, J., Mayr, W., Technology and long-term application of an epineural electrode, Trans. Am. Soc. Artif. Int. Organs, 35 (1989) 490-494.

[25.] van den Honert, C.H., Mortimer, J.T., The response of the myelinated nerve fiber to short duration biphasic stimulating currents, Annals of Biomed. Eng., 7 (1979) 117-125.

[26.] Veraart, C., Grill, W.M., Mortimer, J.T. Selective control of muscle activation with a multipolar nerve cuff electrode, IEEE Trans. Biomed. Eng., 40 (1993) 640-653.

[27.] Warman, E.N., Grill, W.M., Durand, D.,Modeling the effects of electric fields on nerve fibers: determining excitation thresholds, IEEE Trans. Biomed. Eng., 39 (1992) 1244-1254.

[28.] Yoshida, K., Horch K., Selective stimulation of peripheral nerve fibers using dual intrafascicular electrodes, IEEE Trans. Biomed. Eng., 40 (1993) 492-494.

[29.] Zimmermann, M., Selective activation of C-fibers., Pflügers Arch., 301 (1968) 329-333.

FIGURE LEGENDS

Figure 1: Models of mammalian myelinated peripheral nerve fibers. **A.** Model of a single node of Ranvier including the non-linear sodium conductance, g_{Na+}, the sodium Nernst battery, E_{Na+}, the linear leakage conductance g_L, the leak Nernst battery, E_L, and the membrane capacitance, C_m. **B.** Cable model of a myelinated nerve fiber was positioned in the extracellular potentials, $V_e(n)$, generated by a point source electrode. Each node of Ranvier was modeled using the circuit of **A**, and the nodes were connected intracellularly by the axial conductance, G_a.

Figure 2: Transmembrane voltage response of a space-clamped patch of nodal membrane subject to the two-pulse paradigm. The applied current, shown below each trace, consisted of a depolarizing pre-pulse with amplitude equal to 90% of threshold for a 500μsec stimulus followed by a 100μsec stimulus pulse a delays of 0 (**A**), 200μsec (**B**), 400μsec (**C**), and 1000μsec (**D**) after the onset of the 500μsec pre-pulse. The stimulus amplitude (1460μA/cm^2) was the same for all traces.

Figure 3: Effect of pre-pulse and stimulus pulse parameters on the increase in threshold generated by the depolarizing pre-pulse. **A.** Change in threshold, expressed as a percentage of the threshold without any pre-pulse, as a function of the stimulus pulsewidth for different duration depolarizing pre-pulses with amplitudes equal to 95% of threshold. **B.** Change in threshold generated by a 500μsec depolarizing pre-pulse, expressed as a percentage of the threshold without any pre-pulse, as a function of the amplitude of the pre-pulse. **C.** Change in threshold generated by a 500μsec depolarizing pre-pulse with amplitude equal to 95% of threshold, expressed as a percentage of the threshold without any pre-pulse, as a function of the delay between the end of the pre-pulse and the onset of a 500μsec stimulus pulse.

Figure 4: Experimental measurements of the effect of pre-pulse parameters on threshold for excitation of cat sciatic nerve motor fibers. **A.** Threshold for a 500μsec stimulus pulse, expressed

as a percentage of threshold measured without any pre-pulse, as a function of the duration of a depolarizing pre-pulse with amplitude equal to 95% of the excitation threshold at each pre-pulse duration. **B.** Threshold for a 500μsec stimulus pulse, expressed as a percentage of threshold measured without any pre-pulse, as a function of the amplitude of a 500μsec depolarizing pre-pulse.

Figure 5: Transmembrane potential, V_m, and the values of the sodium channel gating parameters, **h** and **m**, as a function of time generated by a sub-threshold depolarizing pre-pulse followed by a 100μsec stimulus pulse at 100μsec (**A**) and 400μsec (**B**) after the onset of the pre-pulse. The arrow in each cases illustrates the onset time of the stimulus pulse.

Figure 6: Transmembrane voltage response of model myelinated nerve fibers positioned 0.25mm and 0.5mm from a point source stimulating electrode. The applied current was a 500μsec pre-pulse at 90% of the closer fiber's threshold followed by a 500μsec stimulus pulse that was supra-threshold for the fiber at 0.5mm. Each trace is the transmembrane potential at that node as a function of time. The stimulus pulse generated a propagating action potential in the fiber at 0.5mm, but not in the fiber at 0.25mm.

Figure 7: Threshold current as a function of the distance between the point source electrode and 10μm and 20μm model nerve fibers. **A.** Current-distance relationship for a monophasic 500μsec stimulus pulse. **B.** Current-distance relationship for a monophasic 500μsec stimulus pulse preceded by a 500μsec depolarizing pre-pulse with amplitude equal to 95% of the threshold for activation of a 20μm fiber positioned 0.25mm from the electrode. **C.** Current-distance relationship for a monophasic 500μsec stimulus pulse preceded by a double 500μsec depolarizing pre-pulse. The amplitude of the first phase was equal to 95% of the threshold for activation of a 20μm fiber positioned 0.25mm from the electrode, and the amplitude of the second phase was equal to 95% of

the threshold for activation of a 20μm fiber positioned 0.5mm from the electrode after the first step of the pre-pulse.

Figure 8: Experimental measurement of the effect of a 500μsec depolarizing pre-pulse on the recruitment of cat sciatic nerve fascicles. **A.** Recruitment curve of the peak plantarflexion/dorsiflexion ankle joint torque as a function of stimulus current amplitude of a 500μsec stimulus pulse or a 500μsec pre-pulse followed by a 500μsec stimulus pulse. **B.** Traces of the ensemble average of 10 torque twitches generated by the indicated stimulus amplitude, either with or without a 500μsec pre-pulse. With a 500μsec stimulus pulse plantarflexion torque was generated first as shown by the positive deflection of the recruitment curves and the positive going twitches. However, when the stimulus was preceded by a 500μsec pre-pulse, dorsiflexion torque was generated first as shown by the negative deflection in the recruitment curves and the negative going twitches.

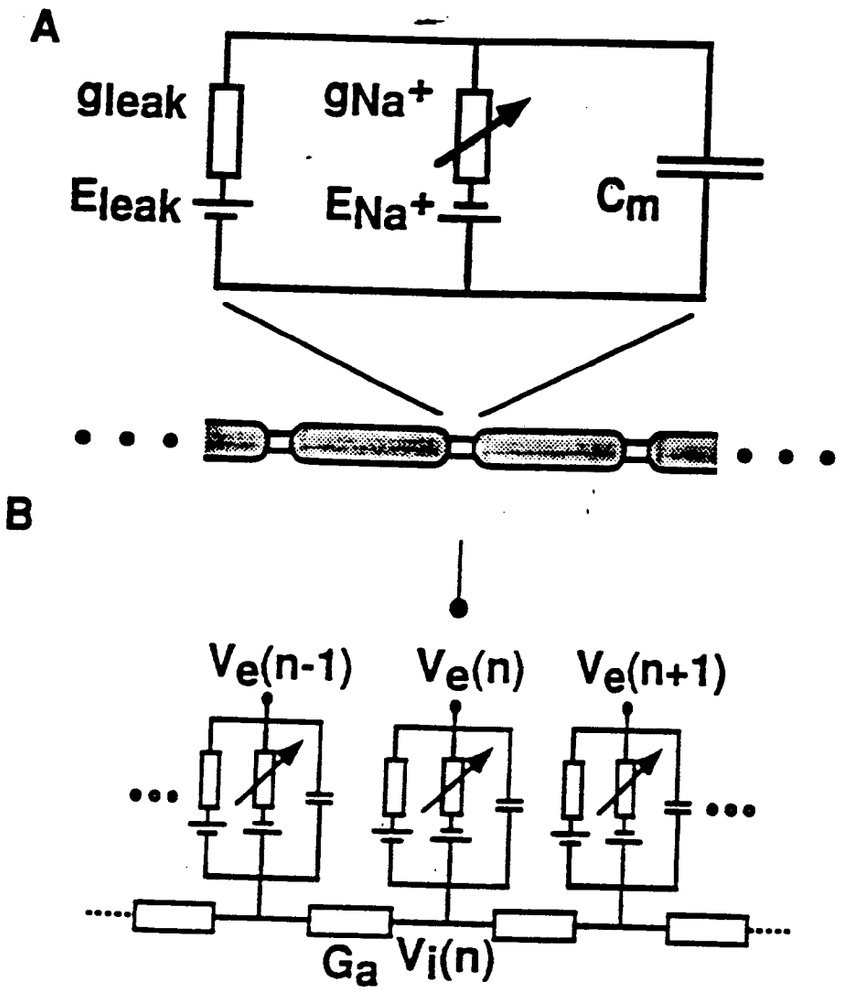

Figure 1

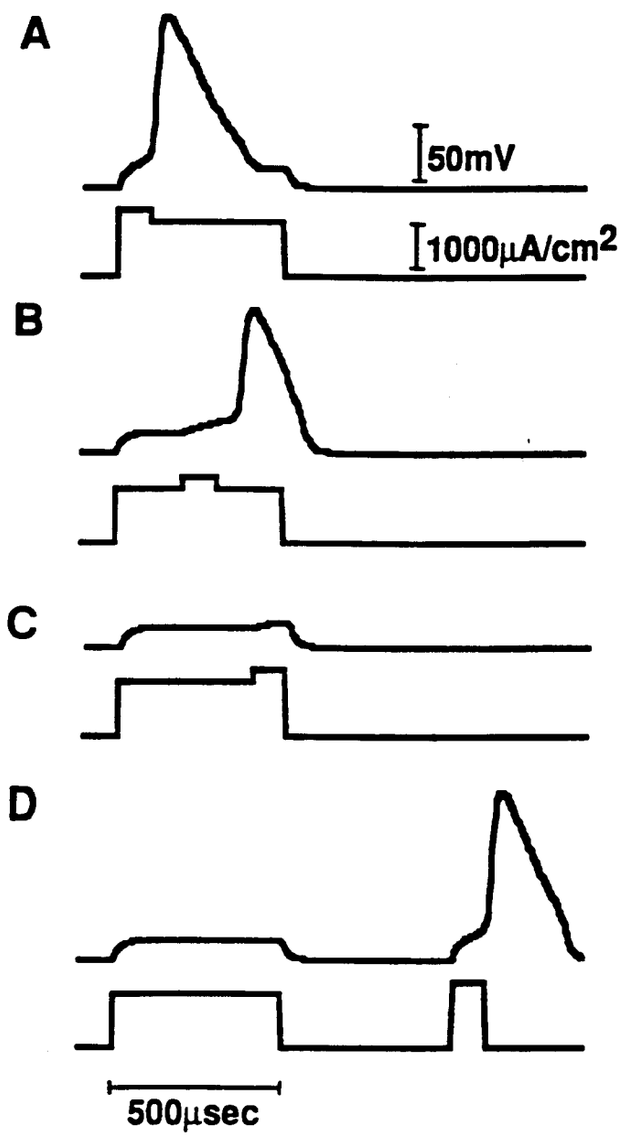

Figure 2

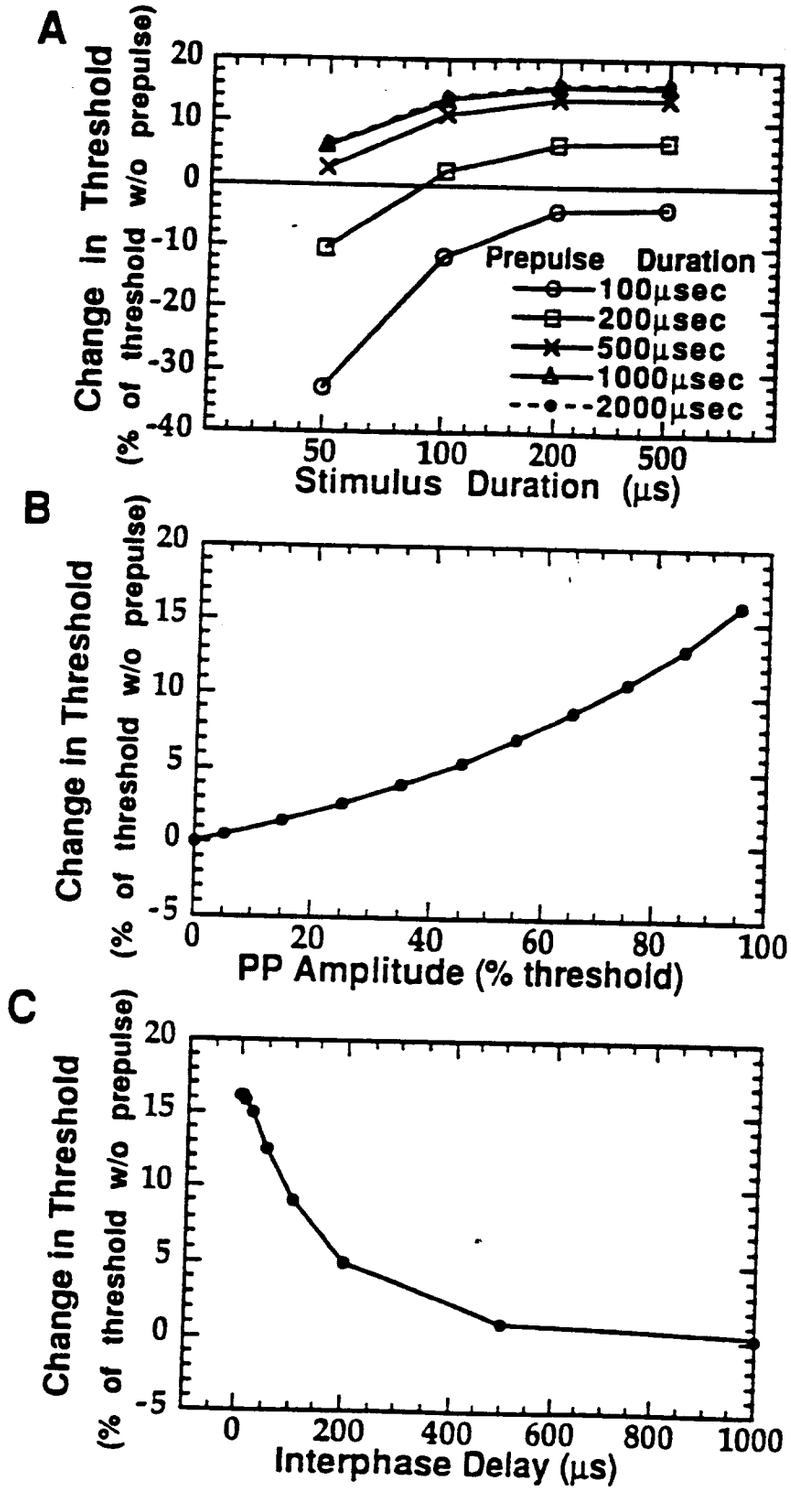
A
Change in Threshold (% of threshold w/o prepulse)
20
10
0
-10
-20
-30
-40
Prepulse Duration
100µsec
200µsec
500µsec
1000µsec
2000µsec
50
100
200
500
Stimulus Duration (µs)
B
Change in Threshold (% of threshold w/o prepulse)
20
15
10
5
0
-5
0
20
40
60
80
100
PP Amplitude (% threshold)
C
Change in Threshold (% of threshold w/o prepulse)
20
15
10
5
0
-5
0
200
400
600
800
1000
Interphase Delay (µs)

Figure 3

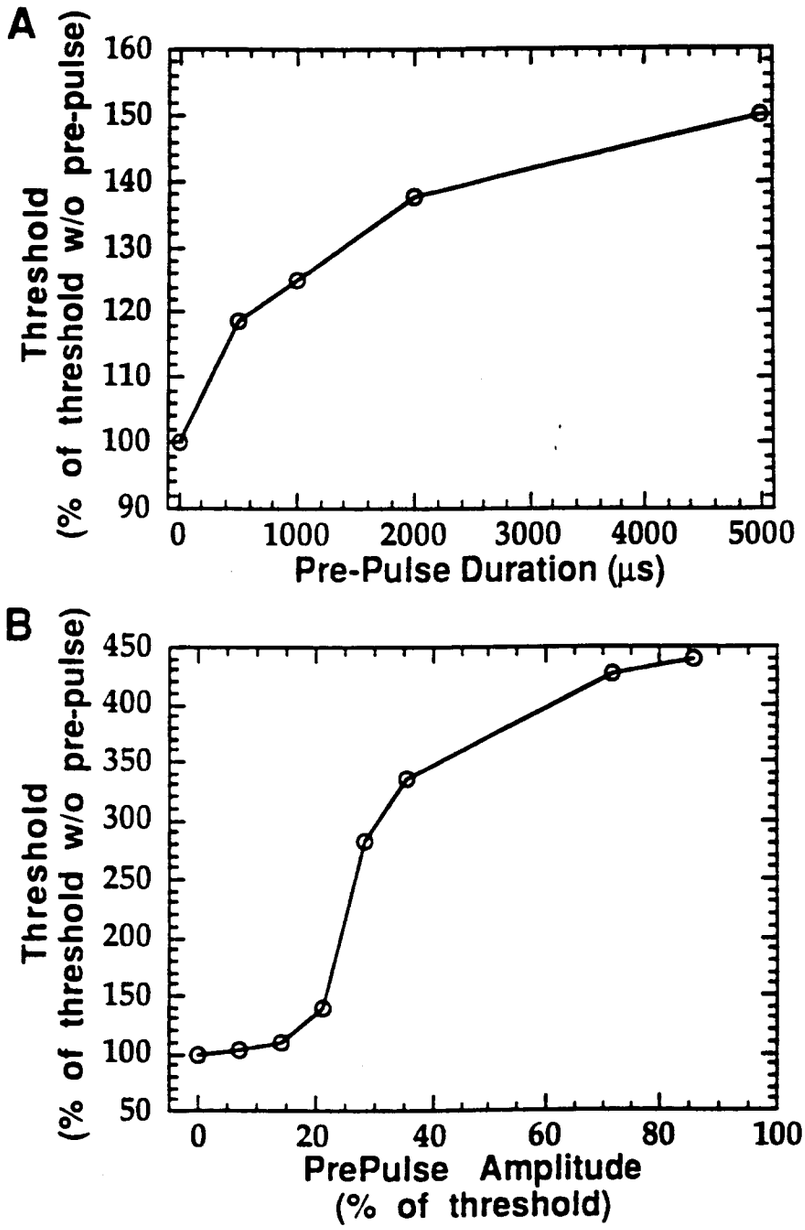
A
Threshold
(% of threshold w/o pre-pulse)
160
150
140
130
120
110
100
90
0
1000
2000
3000
4000
5000
Pre-Pulse Duration (μs)
B
Threshold
(% of threshold w/o pre-pulse)
450
400
350
300
250
200
150
100
50
0
20
40
60
80
100
PrePulse Amplitude
(% of threshold)

Figure 4

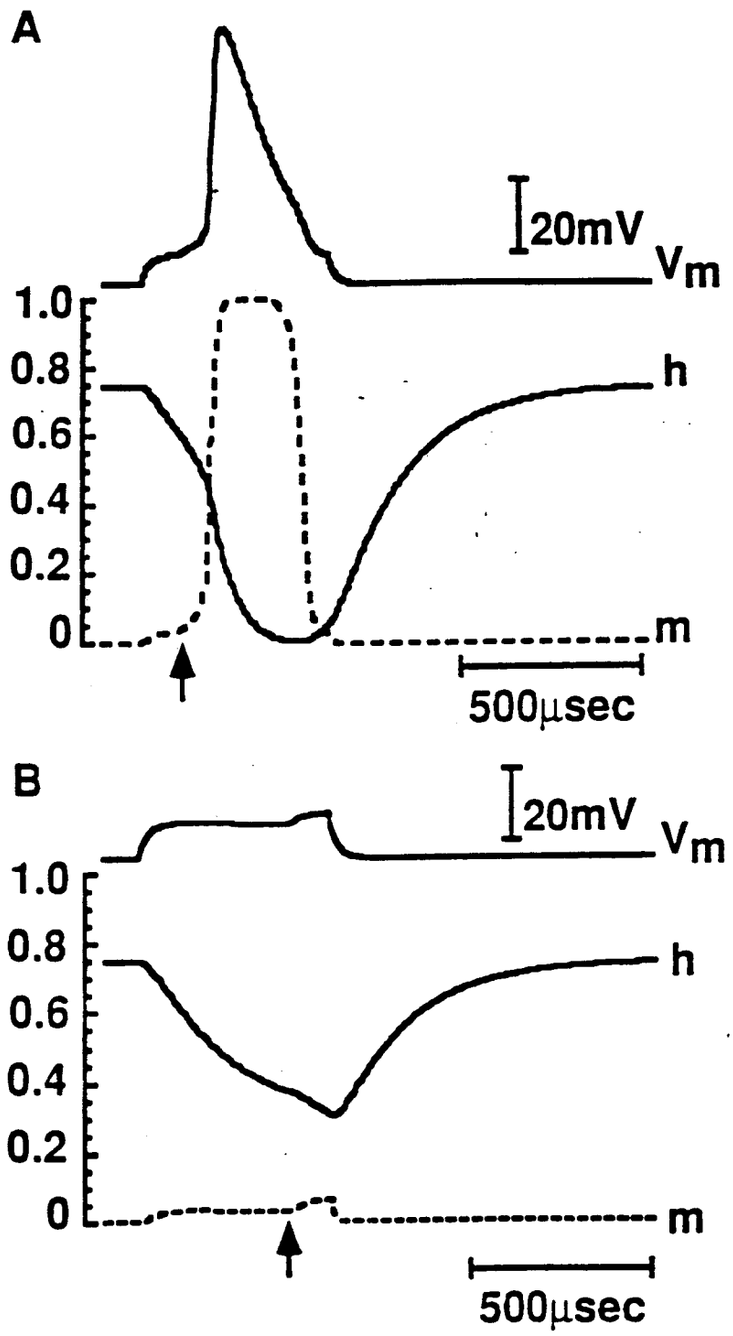
A
20mV
Vm
1.0
0.8
0.6
0.4
0.2
0
h
m
500μsec
B
20mV
Vm
1.0
0.8
0.6
0.4
0.2
0
h
m
500μsec

Figure 5

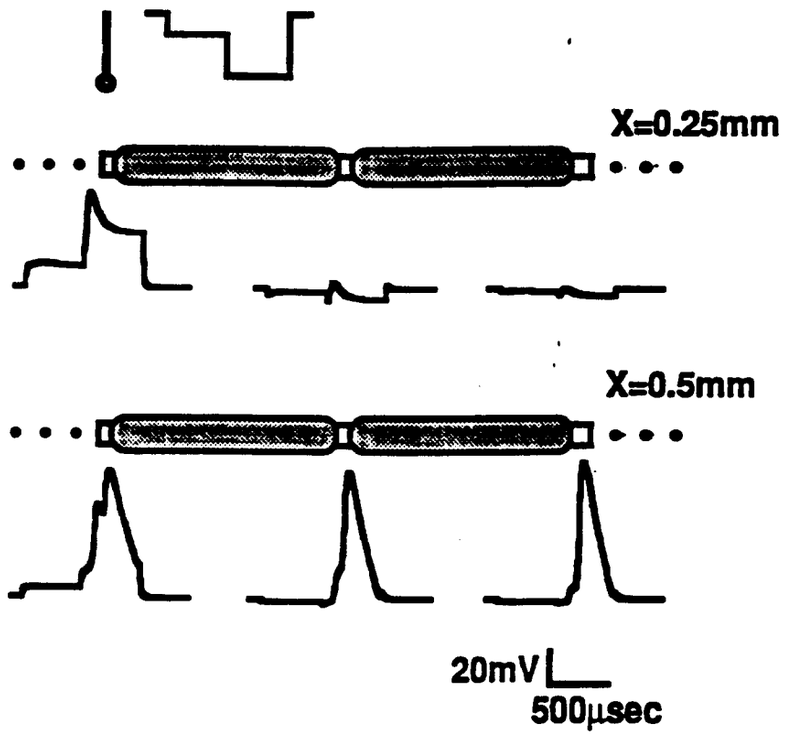

Figure 6

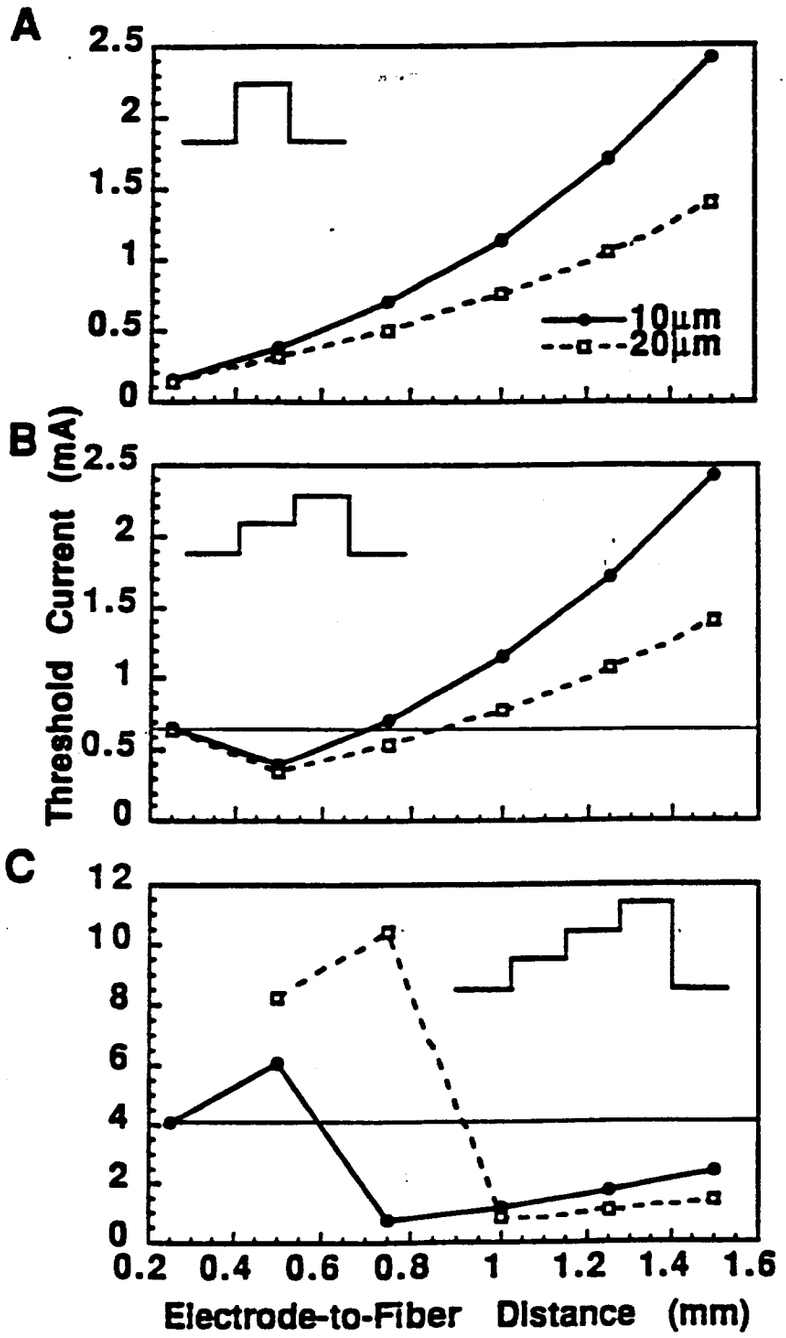
A
2.5
2
1.5
1
0.5
0
10µm
20µm
B
Threshold Current (mA)
2.5
2
1.5
1
0.5
0
C
12
10
8
6
4
2
0
0.2
0.4
0.6
0.8
1
1.2
1.4
1.6
Electrode-to-Fiber Distance (mm)

Figure 7

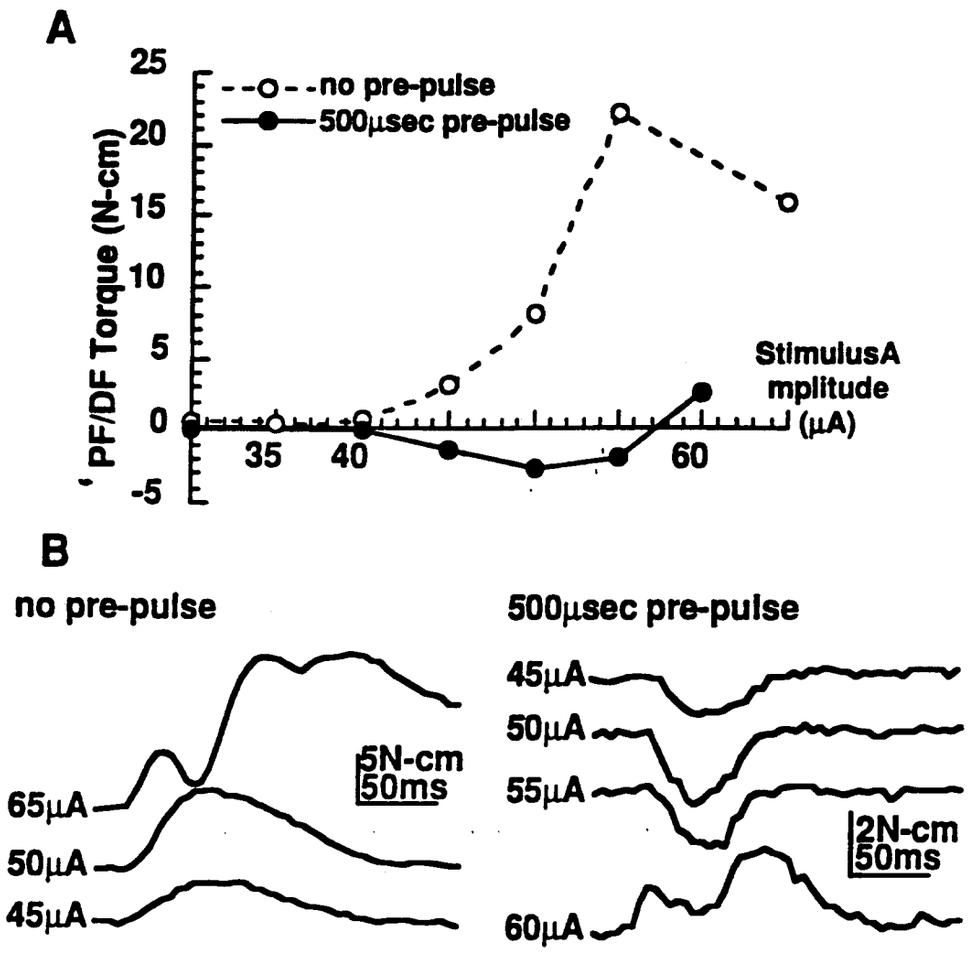
A
25
20
15
10
5
0
-5
PF/DF Torque (N-cm)
no pre-pulse
500µsec pre-pulse
35
40
60
StimulusAmplitude (µA)
B
no pre-pulse
500µsec pre-pulse
65µA
50µA
45µA
5N-cm
50ms
45µA
50µA
55µA
60µA
2N-cm
50ms

Figure 8